Inorg. Chem. **2005**, *44*, 6632–6640

Investigation of the Crystal Structure and the Structural and Magnetic Properties of $SrCu_2(PO_4)_2$

Alexei A. Belik,*[,†,‡] Masaki Azuma,[‡,§] Akira Matsuo,[||,@] Myung-Hwan Whangbo,[⊥] Hyun-Joo Koo,[#] Jun Kikuchi,[£] Tomoyuki Kaji,[|] Susumu Okubo,[¢,+] Hitoshi Ohta,[¢,+] Koichi Kindo,[||,@] and Mikio Takano[‡]

International Center for Young Scientists, National Institute for Materials Science, Namiki 1-1, Tsukuba, Ibaraki, 305-0044, Japan, Institute for Chemical Research, Kyoto University, Uji, Kyoto-fu 611-0011, Japan, PRESTO, Japan Science and Technology Corporation (JST), Kawaguchi, Saitama 332-0012, Japan, KYOKUKEN, Osaka University, Toyonaka, Osaka 560-8531, Japan, Department of Chemistry, North Carolina State University, Raleigh, North Carolina 27695-8204, Department of Chemistry and Institute of Basic Science, Kyung Hee University, Seoul 130-701, South Korea, Division of New Material Sciences, Institute for Solid State Physics, University of Tokyo, 5-1-5 Kashiwanoha, Kashiwa, Chiba 277-8581, Japan, The Graduate School for Science and Technology, Kobe University, Kobe 657-8501, Japan, Molecular Photoscience Research Center, Kobe University, Kobe 657-8501, Japan, and Venture Business Laboratory, Kobe University, Kobe 657-8501, Japan

Received June 29, 2005

$SrCu_2(PO_4)_2$ was prepared by the solid-state method at 1153 K. Its structure was solved by direct methods in the space group *Pccn* (No. 56) with $Z = 8$ from synchrotron X-ray powder diffraction data measured at room temperature. Structure parameters were then refined by the Rietveld method to obtain the lattice parameters, $a = 7.94217(8)$ Å, $b = 15.36918(14)$ Å, and $c = 10.37036(10)$ Å. $SrCu_2(PO_4)_2$ presents a new structure type and is built up from Sr_2O_{16} and $Cu1Cu2O_8$ units with Cu1···Cu2 = 3.256 Å. The magnetic properties of $SrCu_2(PO_4)_2$ were investigated by magnetic susceptibility, magnetization up to 65 T, Cu nuclear quadrupole resonance (NQR), electron-spin resonance, and specific heat measurements. With spin-dimer analysis, it was shown that the two strongest spin-exchange interactions between Cu sites result from the Cu1–O···O–Cu2 and Cu2–O···O–Cu2 super-superexchange paths with Cu1···Cu2 = 5.861 Å and Cu2···Cu2 = 5.251 Å, and the superexchange associated with the structural dimer $Cu1Cu2O_8$ is negligible. The magnetic susceptibility data were analyzed in terms of a linear four-spin cluster model, Cu1–Cu2–Cu2–Cu1 with $-2J_1/k_B = 82.4$ K for Cu1–Cu2 and $-2J_2/k_B = 59$ K for Cu2–Cu2. A spin gap deduced from this model ($\Delta/k_B = 63$ K) is in agreement with that obtained from the Cu NQR data ($\Delta/k_B = 65$ K). A one-half magnetization plateau was observed between approximately 50 and 63 T at 1.3 K. Specific heat data show that $SrCu_2(PO_4)_2$ does not undergo a long-range magnetic ordering down to 0.45 K. $SrCu_2(PO_4)_2$ melts incongruently at 1189 K. We also report its vibrational properties studied with Raman spectroscopy.

1. Introduction

Low-dimensional quantum-spin systems have received considerable attention during the past decades from both theoretical and experimental points of view.[1] One of the reasons for this interest is to understand the superconducting properties of the two-dimensional copper oxides. In the course of these studies, many low-dimensional magnetic systems with a spin-singlet ground state have been discovered (e.g., the $S = 1/2$ alternating chain compound $(VO)_2P_2O_7$,[2,3] the $S = 1/2$ two-leg ladders $SrCu_2O_3$[4] and $Sr_{14}Cu_{24}O_{41}$,[5] the

* To whom correspondence should be addressed. International Center for Young Scientists, National Institute for Materials Science, Namiki 1-1, Tsukuba, Ibaraki, 305-0044, Japan. E-mail: Alexei.BELIK@nims.go.jp.
† International Center for Young Scientists, National Institute for Materials Science.
‡ Institute for Chemical Research, Kyoto University.
§ PRESTO, Japan Science and Technology Corporation (JST).
|| KYOKUKEN, Osaka University.
⊥ Department of Chemistry, North Carolina State University.
Department of Chemistry and Institute of Basic Science, Kyung Hee University.
£ Division of New Material Sciences, Institute for Solid State Physics, University of Tokyo.
| The Graduate School for Science and Technology, Kobe University.
¢ Molecular Photoscience Research Center, Kobe University.
+ Venture Business Laboratory, Kobe University.
@ Current address: Institute for Solid State Physics, University of Tokyo, Kashiwanoha 5-1-5, Kashiwa, Chiba 277-8581, Japan.

(1) Lemmens, P.; Güntherodt, G.; Gros, C. *Phys. Rep.* **2003**, *375*, 1.
(2) (a) Azuma, M.; Saito, T.; Fujishiro, Y.; Hiroi, Z.; Takano, M.; Izumi, F.; Kamiyama, T.; Ikeda, T.; Narumi, Y.; Kindo, K. *Phys. Rev. B* **1999**, *60*, 10145. (b) Kikuchi, J.; Motoya, K.; Yamauchi, T.; Ueda, Y. *Phys. Rev. B* **1999**, *60*, 6731.
(3) Koo, H.-J.; Whangbo, M.-H.; VerNooy, P. D.; Torardi, C. C.; Marshall, W. J. *Inorg. Chem.* **2002**, *41*, 4664−4672.
(4) (a) Hiroi, Z.; Azuma, M.; Takano, M.; Bando, Y. *J. Solid State Chem.* **1991**, *95*, 230. (b) Azuma, M.; Hiroi, Z.; Takano, M.; Ishida, K.; Kitaoka, Y. *Phys. Rev. Lett.* **1994**, *73*, 3463.
(5) Eccleston, R. S.; Uehara, M.; Akimitsu, J.; Eisaki, H.; Motoyama, N.; Uchida, S. I. *Phys. Rev. Lett.* **1998**, *81*, 1702.

10.1021/ic051079h CCC: $30.25
Published on Web 08/25/2005

$S = 1$ chains Y_2BaNiO_5[6] and $PbNi_2V_2O_8$[7] (Haldane systems), the spin-Peierls compound $CuGeO_3$,[8] and $CaCuGe_2O_6$[9] with weakly interacting dimer units). An important compound bridging the one- and two-dimensional magnetic properties is the spin-frustrated system $SrCu_2(BO_3)_2$,[1,10] which does not show a long-range magnetic ordering but has a spin gap of about 30 K with several quantized magnetization plateaus.[10]

Recently, it was shown that $SrCu_2(PO_4)_2$ has a singlet ground state and a spin gap in the excitation spectrum.[11] $SrCu_2(PO_4)_2$ was regarded[11] as isotypic with $BaCu_2(PO_4)_2$[12] (space group $P\bar{1}$). However, our previous work showed that $SrCu_2(PO_4)_2$ crystallizes in an orthorhombic system.[13] Information about the structure is essential for interpreting the magnetic properties correctly. In the present work, we report the crystal structure of $SrCu_2(PO_4)_2$, determined by direct methods from synchrotron X-ray powder diffraction (XRD) data. We characterize this compound by magnetic susceptibility, magnetization up to 65 T, Cu nuclear quadrupole resonance (NQR), electron-spin resonance (ESR), specific heat, thermal analysis, Raman spectroscopy, and spin-dimer analysis. Magnetic susceptibilities demonstrate the typical behavior for gapped low-dimensional Heisenberg antiferromagnets. $SrCu_2(PO_4)_2$ does not show long-range magnetic ordering down to 0.45 K. Although the crystal structure of $SrCu_2(PO_4)_2$ consists of the structural dimers $Cu1Cu2O_8$ with $Cu1\cdots Cu2 = 3.256$ Å, the magnetic properties of $SrCu_2(PO_4)_2$ are described by a linear four-spin cluster model whose spin-exchange paths do not include the structural dimer.

2. Experimental Section

Synthesis. $SrCu_2(PO_4)_2$ was synthesized by the solid-state method from stoichiometric mixtures of $Sr_3(PO_4)_2$ and $Cu_3(PO_4)_2$ at 1153 K in a Pt crucible for 200 h with five intermediate grindings. The green-blue product was cooled in a furnace. $SrCu_2(PO_4)_2$ contained $Sr_3Cu_3(PO_4)_4$ (1.2%) impurities.[13] The mass fraction of the impurity in the sample was calculated from the scale factors refined in the Rietveld analysis described below.

Single-phased $Cu_3(PO_4)_2$ and $Sr_3(PO_4)_2$ were prepared from mixtures of CuO (99.99%), $NH_4H_2PO_4$ (99.999%), and $SrCO_3$ (99.999%) by the solid-state method. The mixtures were heated under air while the temperature was very slowly increased from room temperature (RT) to 873 K; then, they were reground and allowed to react at 1153 K for $Cu_3(PO_4)_2$, and 1273 K for $Sr_3(PO_4)_2$ for 120 h with four intermediate grindings.

XRD Experiments, Structure Solution, and Structure Refinements by the Rietveld Method. The XRD data for phase analysis were measured at RT on a RIGAKU RINT 2500 Bragg−Brentano-type powder diffractometer operated at 40 kV and 300 mA (Cu Kα radiation). The XRD data were collected in a 2θ range of 5 to 80° with a step width of 0.02° and a counting time of 1 s/step.

Synchrotron XRD data of $SrCu_2(PO_4)_2$ for the structure solution and refinement were measured at RT on a powder diffractometer BL02B2 at SPring-8 with Debye−Scherrer geometry.[14] The incident beam from a bending magnet was monochromatized to $\lambda = 0.77572$ Å. The sample was contained in a glass capillary tube with an inner diameter of 0.2 mm and rotated during measurements. The synchrotron XRD data were collected in a 2θ range from 1 to 75° with a step interval of 0.01° for 60 min.

The structure of $SrCu_2(PO_4)_2$ was solved ab initio by direct methods from the synchrotron XRD data with EXPO[15] using the program's default settings. The structural parameters of $SrCu_2(PO_4)_2$ were refined by the Rietveld method from the synchrotron XRD data using RIETAN-2000.[16] The split pseudo-Voigt function of Toraya[17] was used as a profile function. The background was represented by a composite background function (i.e., the 11th order Legendre polynomial multiplied by a set of numerical values to approximate the background). The coefficients for the analytical approximation to the atomic scattering factors for Sr, Cu, P, and O were taken from ref 18. Isotropic atomic displacement parameters, B, with the isotropic Debye−Waller factor represented as $\exp(-B\sin^2\theta / \lambda^2)$ were assigned to all the sites.

Physical and Chemical Characterization. The magnetic susceptibilities, $\chi(T)$, of $SrCu_2(PO_4)_2$ were measured on a DC SQUID magnetometer (Quantum Design, MPMS XL) between 2 and 400 K in applied fields of 100 and 5000 Oe (1 Oe = $(10^3/4\pi)$ Am^{-1}) under both zero-field-cooled (ZFC) and field-cooled (FC) conditions. The specific heat, $C_p(T)$, was recorded between 0.45 and 51 K, on cooling, by a pulse relaxation method using a commercial calorimeter (Quantum Design PPMS). High-field magnetization data were taken at 1.3 and 4.2 K in a pulsed magnetic field up to 65 T by an induction method using a multilayer pulse magnet at KYOKUGEN, Osaka University.

The Cu NQR spectra were taken under zero external field by integrating the spin-echo signal while changing the frequency point by point. The nuclear spin lattice relaxation rate was measured by an inversion recovery method.

The X-band (9.5 GHz) ESR measurements were performed using a Bruker ESR spectrometer (EMX081) with a TE_{103} rectangular cavity and an Oxford He flow cryostat (ESR900) at the Venture Business Laboratory of Kobe University. High-field ESR measurements were done using Gunn oscillators at 80, 160, and 315 GHz with the pulsed magnetic field up to 16 T at Kobe University.

Unpolarized Raman spectra of $SrCu_2(PO_4)_2$ were collected at RT with a micro Raman spectrometer (Horiba Jobin-Yvon T64000) in backscattering geometry with a CCD detector. Raman scattering was excited using an Ar^+ laser at a wavelength of 514.5 nm.

The thermal stability of $SrCu_2(PO_4)_2$ was examined under air with a MacScience TG-DTA 2000 instrument. The sample was placed in a Pt crucible, heated to 1223 K, and then cooled at a rate of 10 K/min. Differential thermal analysis (DTA) data showed one

(6) Darriet, J.; Regnault, L. P. *Solid State Commun.* **1993**, *86*, 409.
(7) Uchiyama, Y.; Sasago, Y.; Tsukada, I.; Uchinokura, K.; Zheludev, A.; Hayashi, T.; Miura, N.; Böni, P. *Phys. Rev. Lett.* **1999**, *83*, 632.
(8) Hase, M.; Terasaki, I.; Uchinokura, K. *Phys. Rev. Lett.* **1993**, *70*, 3651.
(9) Valentí, R.; Saha-Dasgupta, T.; Gros, C. *Phys. Rev. B* **2002**, *66*, 054426.
(10) Kageyama, H.; Yoshimura, K.; Stern, R.; Mushnikov, N. V.; Onizuka, K.; Kato, M.; Kosuge, K.; Slichter, C. P.; Goto, T.; Ueda, Y. *Phys. Rev. Lett.* **1999**, *82*, 3168.
(11) Mekata, M.; Hanabata, T.; Nakaya, K.; Ajiro, Y. *J. Magn. Magn. Mater.* **2001**, *226−230*, 410.
(12) Moqine, A.; Boukhari, A.; Darriet, J. *J. Solid State Chem.* **1993**, *107*, 362.
(13) Belik, A. A.; Malakho, A. P.; Lazoryak, B. I.; Khasanov, S. S. *J. Solid State Chem.* **2002**, *163*, 121.
(14) Nishibori, E.; Takata, M.; Kato, K.; Sakata, M.; Kubota, Y.; Aoyagi, S.; Kuroiwa, Y.; Yamakata, M.; Ikeda, N. *Nucl. Instrum. Methods Phys. Res. Sect. A* **2001**, *467−468*, 1045.
(15) Altomare, A.; Burla, M. C.; Camalli, M.; Carrozzini, B.; Cascarano, G. L.; Giacovazzo, C.; Guagliardi, A.; Moliterni, A. G. G.; Polidori, G.; Rizzi, R. *J. Appl. Crystallogr.* **1999**, *32*, 339.
(16) Izumi, F.; Ikeda, T. *Mater. Sci. Forum* **2000**, *321−324*, 198.
(17) Toraya, H. *J. Appl. Crystallogr.* **1990**, *23*, 485.
(18) *International Tables for Crystallography*, Vol. C, 2nd ed.; Wilson, A. J. C., Prince, E., Eds.; Kluwer: Dordrecht, The Netherlands, 1999; pp 572−574.

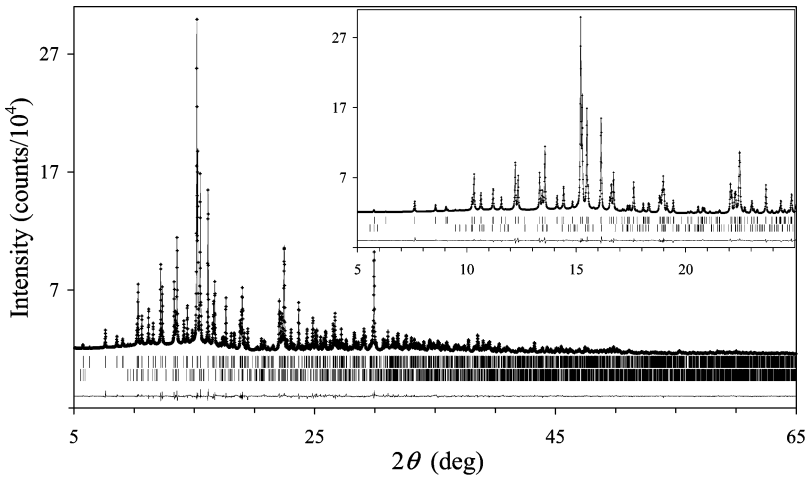

Figure 1. Observed (crosses), calculated (solid line), and difference synchrotron XRD patterns for $SrCu_2(PO_4)_2$. Bragg reflections are indicated by tick marks for $SrCu_2(PO_4)_2$ (upper) and $Sr_3Cu_3(PO_4)_4$ (lower).

peak centered at 1198 K with a shoulder on heating and one broad peak centered at 1169 K on cooling (see Supporting Information). This discrepancy between the heating and cooling behaviors suggested that $SrCu_2(PO_4)_2$ melts incongruently above 1189 K.

3. Results and Discussion

3.1. Structure Analysis of $SrCu_2(PO_4)_2$. Reflections on the synchrotron XRD pattern of $SrCu_2(PO_4)_2$ could be indexed in an orthorhombic system with the lattice parameters $a \approx 7.94$ Å, $b \approx 15.37$ Å, and $c \approx 10.37$ Å, which are similar to those previously reported for $SrCu_2(PO_4)_2$ (described as $Sr_{1.9}Cu_{4.1}(PO_4)_4$ in ref 13). With these lattice parameters, the reflection conditions derived from the indexed reflections were $l = 2n$ for $0kl$ and $h0l$, $h + k = 2n$ for $hk0$, $h = 2n$ for $h00$, $k = 2n$ for $0k0$, and $l = 2n$ for $00l$, which lead to the centrosymmetric space group *Pccn* (No. 56),[19] in agreement with the results of the second-harmonic generation studies for $SrCu_2(PO_4)_2$.[13]

The structure of $SrCu_2(PO_4)_2$ was successfully solved in space group *Pccn* assuming $Z = 8$. With the EXTRA routine,[20] which uses the Le Bail method,[21] 159 independent reflections were extracted from the synchrotron XRD pattern in the 2θ range of 5 to 40°. Fourteen independent atomic positions (one Sr, two Cu, three P, and eight O) were located from the E map with the SIRPOW97 routine.[22] The structural parameters of $SrCu_2(PO_4)_2$ were then refined using the Rietveld method.

Figure 1 shows the experimental, calculated, and difference synchrotron XRD patterns for $SrCu_2(PO_4)_2$. Table 1 lists the experimental and refinement conditions, as well as the lattice parameters and *R* factors. The structural parameters are given in Table 2, and selected bond lengths and bond angles are listed in Table 3.

Table 1. Conditions of the Synchrotron XRD Experiments and Parts of the Refinement Conditions and Results for $SrCu_2(PO_4)_2$

2θ range (deg)	5−65
scan width (deg)	0.01
space group	*Pccn* (No. 56)
Z	8
lattice parameters	
a (Å)	7.94217(8)
b (Å)	15.36918(14)
c (Å)	10.37036(10)
V (Å^3)	1265.85(2)
no of Bragg reflns	1756
variables	
structure, lattice	51, 3
background, profile	12, 10
peak shift, scale	1, 1
R_{wp}, R_p	1.63%, 1.15%
R_B, R_F	1.92%, 1.34%
$S = R_{wp}/R_e$	2.45

Table 2. Fractional Coordinates and Isotropic Atomic Displacement Parameters for $SrCu_2(PO_4)_2$

atom[a]	Wyckoff position	x	y	z	B (Å^2)
Sr	8e	0.02427(11)	−0.12422(7)	−0.08783(11)	1.22(3)
Cu1	8e	0.42917(15)	0.16572(8)	−0.05072(11)	0.95(3)
Cu2	8e	0.91599(15)	0.08222(8)	−0.28762(11)	1.58(3)
P1	4d	0.75	0.25	−0.1718(4)	0.54(8)
P2	8e	0.2052(3)	−0.00920(15)	−0.4284(3)	0.37(6)
P3	4c	0.25	0.25	0.2074(4)	1.50(10)
O11	8e	0.7444(6)	0.1682(3)	−0.2563(6)	0.42(15)
O12	8e	0.5889(6)	0.2564(3)	−0.0887(5)	0.10(12)
O21	8e	0.8842(6)	0.0327(3)	−0.1152(5)	0.5 [b]
O22	8e	0.6490(6)	0.0807(4)	0.0223(5)	0.14(12)
O23	8e	0.0884(7)	−0.0057(3)	−0.3112(5)	0.42(13)
O24	8e	0.2287(5)	0.0781(4)	−0.4998(5)	0.37(14)
O31	8e	0.3986(10)	0.2208(4)	0.1224(6)	3.2(2)
O32	8e	0.3151(6)	0.3287(3)	0.2835(6)	0.84(14)

[a] The occupancies of all of the sites are 1. [b] Fixed values.

The P−O, Cu−O, and Sr−O bond lengths, as well as the atomic displacement parameters, are reasonable. These and the sufficiently low *R* factors indicate that the structure model for $SrCu_2(PO_4)_2$ is correct. In addition, the bond valence sum, *V*,[23] of each atom (see Supporting Information) is in agreement with the formal oxidation state; this also confirms the structure model.

(19) *International Tables for Crystallography*, Vol. A, 5th ed.; Hahn, T., Ed.; Kluwer: Dordrecht, The Netherlands, 2002; p 52.
(20) Altomare, A.; Burla, M. C.; Cascarano, G.; Giacovazzo, C.; Guagliardi, A.; Moliterni, A. G. G.; Polidori, G. *J. Appl. Crystallogr.* **1995**, *28*, 842.
(21) Le Bail, A.; Duroy, H.; Fourquet, J. L. *Mater. Res. Bull.* **1988**, *23*, 447.
(22) Altomare, A.; Cascarano, G.; Giacovazzo, C.; Guagliardi, A.; Burla, M. C.; Polidori, G.; Camalli, M. *J. Appl. Crystallogr.* **1994**, *27*, 435.
(23) Brown, I. D.; Altermatt, D. *Acta Crystallogr., Sect. B* **1985**, *41*, 244.

Table 3. Bond Lengths, l (Å), and Angles, ϕ (deg), in $SrCu_2(PO_4)_2$

Sr−O11	2.475(5)
Sr−O31	2.607(6)
Sr−O24	2.615(4)
Sr−O21	2.634(5)
Sr−O12	2.642(5)
Sr−O21′	2.671(5)
Sr−O32	2.720(6)
Sr−O22	2.765(5)
Sr−O23	2.991(5)
Cu1−O24	1.914(5)
Cu1−O12	1.925(5)
Cu1−O32	1.946(6)
Cu1−O31	2.000(6)
Cu1−O22	2.308(5)
Cu1−O23	3.115(5)
Cu2−O11	1.925(5)
Cu2−O23	1.939(5)
Cu2−O21	1.960(5)
Cu2−O22	2.038(5)
Cu2−O31	2.752(6)
Cu2−O23′	3.033(6)
Cu1−O31−Cu2	84.9(2)
Cu1−O22−Cu2	96.9(2)
P1−O11 (×2)	1.533(5)
P1−O12 (×2)	1.546(5)
P2−O21	1.535(5)
P2−O22	1.535(5)
P2−O23	1.530(6)
P2−O24	1.544(5)
P3−O31 (×2)	1.540(7)
P3−O32 (×2)	1.533(5)

$SrCu_2(PO_4)_2$ presents a new structure type among compounds with the stoichiometry of $AM_2(PO_4)_2$ (A = Ca, Sr, Ba, and Pb; M = Mg and transition metals).[12,24−30] The Sr atoms are surrounded by 9 oxygen atoms. Two SrO_9 polyhedra have a common edge (O21−O21) forming isolated Sr_2O_{16} units (Figure 2). The Cu1 and Cu2 atoms are located in strongly distorted square pyramids. The bases of the pyramids are not flat. The apical Cu2−O31 bond is rather long (about 2.8 Å), so the O31 atom can be excluded from the first-coordination sphere of the Cu2 atom. The $Cu1O_{4+1}$ and $Cu2O_4$ polyhedra are jointed by a vertex (O22) forming a structural dimer unit $Cu1Cu2O_8$ (Figures 3 and 4), which provides the Cu−O−Cu superexchange (SE) path with Cu···Cu = 3.256 Å, Cu−O = 2.038 and 2.308 Å, and ∠Cu−O−Cu = 96.8°. The other Cu−O distances are greater than 3.0 Å.

3.2. Vibrational Properties of $SrCu_2(PO_4)_2$. The internal vibrational modes of a free PO_4^{3-} tetrahedron with T_d symmetry are decomposed as $A_1 + E + 2T_2$.[31] The mode with the A_1 symmetry type is the symmetric stretching mode (ν_1) of the P−O bonds. The modes with the E and T_2 symmetry types are the O−P−O bending modes (ν_2 and ν_4, respectively). The second mode with the T_2 symmetry is the asymmetric stretching mode (ν_3). For a free PO_4^{3-} tetrahedron, $\nu_1 = 938$ cm^{-1}, $\nu_2 = 420$ cm^{-1}, $\nu_3 = 1017$ cm^{-1}, and $\nu_4 = 567$ cm^{-1}.[31] The Raman bands in $SrCu_2(PO_4)_2$ are distributed in four distinct wavenumber ranges: 50−380

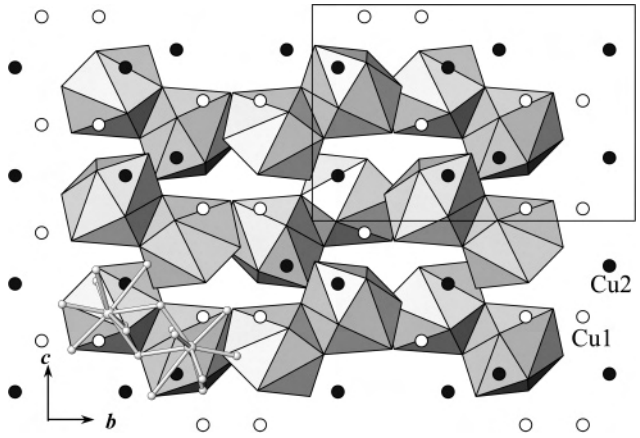

Figure 2. Schematic projection view of the structure of $SrCu_2(PO_4)_2$ along the a axis with polyhedral representation of the Sr_2O_{16} units. The Cu1 and Cu2 atoms are represented by circles. The PO_4 tetrahedra are not shown. For one Sr_2O_{16} unit, the ball-and-stick representations of the Sr−O bonds are given.

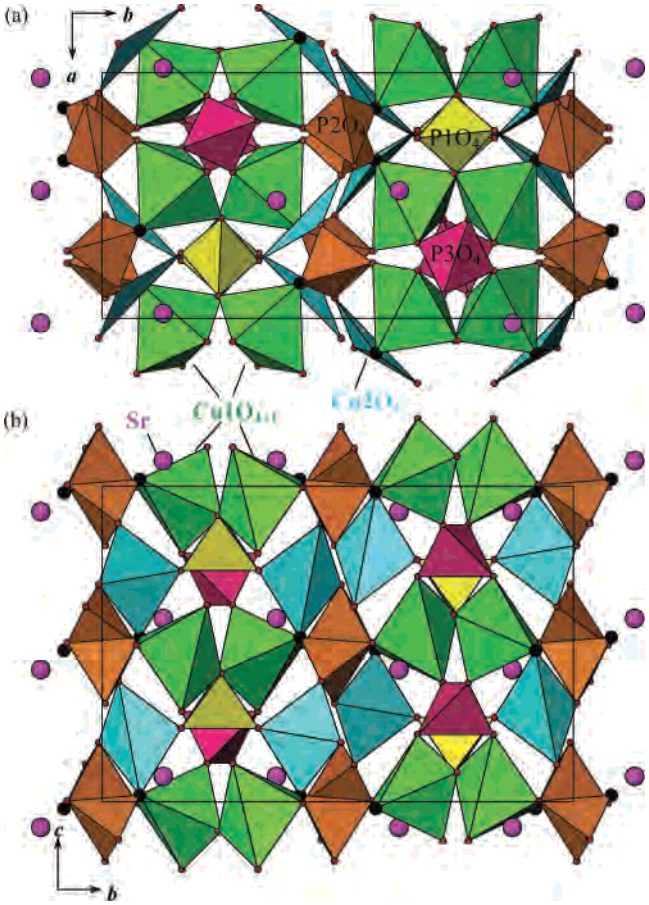

Figure 3. Schematic projection views of the structure of $SrCu_2(PO_4)_2$ along (a) the c axis and (b) the a axis. The $Cu1O_{4+1}$ and $Cu2O_4$ polyhedra (the apical O31 atom was omitted for clarity) and the PO_4 tetrahedra are shown. The Sr atoms are represented by circles. Black circles represent the O22 atoms through which connections in the structural $Cu1Cu2O_8$ dimer occur.

(24) Maass, K.; Glaum, R.; Gruehn, R. *Z. Anorg. Allg. Chem.* **2002**, *628*, 1663.
(25) El-Bali, B.; Boukhari, A.; Glaum, R.; Gerk, M.; Maass, K. *Z. Anorg. Allg. Chem.* **2000**, *626*, 2557.
(26) Elbali, B.; Boukhari, A.; Holt, E. M.; Aride, J. *J. Crystallogr. Spectrosc. Res.* **1993**, *23*, 1001.
(27) Elbali, B.; Boukhari, A.; Aride, J.; Abraham, F. *J. Solid State Chem.* **1993**, *104*, 453.
(28) Hemon, A.; Courbion, G. *J. Solid State Chem.* **1990**, *85*, 164.
(29) Bircsak, Z.; Harrison, W. T. A. *Acta Crystallogr., Sect. C* **1998**, *54*, 1554.
(30) Belik, A. A.; Azuma, M.; Takano, M.; Lazoryak, B. I. *Chem. Mater.* **2004**, *16*, 4311.
(31) de Aza, P. N.; Santos, C.; Pazo, A.; de Aza, S.; Cusco, R.; Artus, L. *Chem. Mater.* **1997**, *9*, 912.

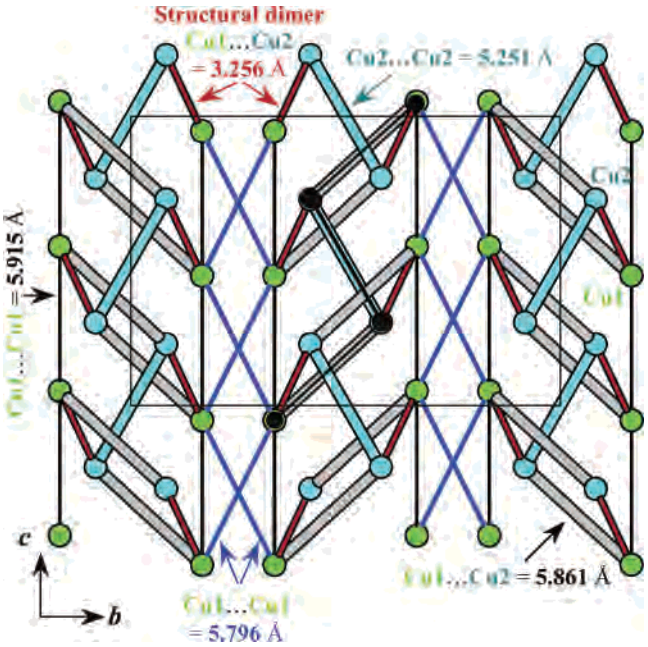

Figure 4. Schematic projection view of the structure of $SrCu_2(PO_4)_2$ along the *a* axis presenting the arrangement of the linear tetramer units, the structural dimers, and the two strongest intertetramer interactions with Cu1···Cu1 = 5.796 Å and Cu1···Cu1 = 5.915 Å (Table 5) which form three-dimensional connections between the tetramers. One linear tetramer cluster is marked by black circles and lines.

cm^{-1}, 380−530 cm^{-1}, 530−710 cm^{-1}, and 870−1400 cm^{-1}. The first range corresponds to the lattice vibrations. The other ranges correspond to the internal modes ν_2, ν_4, and $\nu_1 + \nu_3$ of a free PO_4^{3-} ion, respectively. Group analysis of the internal stretching and bending modes of the PO_4^{3-} groups in $SrCu_2(PO_4)_2$ predicts the following selection rules: $19A_g + 19B_{1g} + 19A_u + 19B_{1u} + 17B_{2g} + 17B_{3g} + 17B_{2u} + 17B_{3u}$. The A_g, B_{1g}, B_{2g}, and B_{3g} modes are Raman active. Therefore, between 380 and 1400 cm^{-1}, 72 Raman bands are expected, while about 25 bands were observed experimentally (see Supporting Information). This fact shows that many of the bands overlap.

3.3. Spin-Dimer Analysis of $SrCu_2(PO_4)_2$. Spin-exchange interactions between the Cu^{2+} ions of $SrCu_2(PO_4)_2$ can occur not only through the SE path Cu−O−Cu but also through the super-superexchange (SSE) path Cu−O···O−Cu, where the O···O contact forms an edge of the PO_4 group coordinating the two Cu atoms. SSE interactions can be rather strong in magnitude (e.g., $-2J/k_B = 143$ K in $Sr_2Cu(PO_4)_2$)[32] and can be even stronger than SE interactions.[33,34] To find spin-structure models appropriate for analyzing the magnetic susceptibility data of $SrCu_2(PO_4)_2$, therefore, it is necessary to examine the relative strengths of the SE and SSE interactions of $SrCu_2(PO_4)_2$. In this section, we estimate these interactions in terms of a spin-dimer analysis on the basis of extended Hückel tight-binding calculations.[33,35]

(32) (a) Belik, A. A.; Azuma, M.; Takano, M. *J. Solid State Chem.* **2004**, *177*, 883. (b) Belik, A. A.; Azuma, M.; Takano, M. *J. Magn. Magn. Mater.* **2004**, *272*−*276*, 937.
(33) Whangbo, M.-H.; Dai D.; Koo H.-J. *Solid State Sci.* **2005**, *7*, 827.
(34) Koo, H.-J.; Dai, D.; Whangbo, M.-H. *Inorg. Chem.* **2005**, *44*, 4359.
(35) Whangbo, M.-H.; Koo, H.-J.; Dai, D. *J. Solid State Chem.* **2003**, *176*, 417.

Table 4. Geometrical Parameters of the SSE Paths of $SrCu_2(PO_4)_2$

Cu···Cu (Å)	Cu−O (Å)	O···O (Å)	∠Cu−O···O (deg)
	(a) Cu1···Cu1		
3.849	1.945, 1.945	2.631	102.9, 102.9
	1.999, 1.999	2.525	105.3, 105.3
5.716	1.925, 1.925	2.567	126.9, 126.9
5.796	1.945, 1.999	2.446	120.5, 158.9
5.915	1.945, 1.999	2.500	156.9, 123.6
	(b) Cu1···Cu2		
4.164	1.914, 2.038	2.532	119.3, 99.4
4.749	1.925, 1.926	2.473	146.7, 93.5
4.757	1.925, 1.926	2.527	94.3, 146.1
5.861	1.959, 1.941	2.418	142.1, 165.0
	(c) Cu2···Cu2		
4.771	1.959, 1.939	2.505	84.7, 144.7
	1.926, 1.939	2.874	75.5, 151.5
5.251	2.038, 1.939	2.520	142.8, 124.3
	1.939, 2.038	2.520	124.3, 142.8
5.792	1.926, 1.926	2.516	131.4, 131.4
5.817	2.038, 1.959	2.463	139.1, 120.6

Table 5. Relative $(\Delta e)^2$ Values Calculated for the SE and SSE Interactions of $SrCu_2(PO_4)_2$ without PO_4 Bridges for the SSE Interactions

	Cu···Cu (Å)	relative $(\Delta e)^2$
	(a) SE	
Cu1···Cu2	3.256	0.00
	(b) SSE	
Cu1···Cu1	3.849	0.10
	5.716	0.06
	5.796	0.32
	5.915	0.23
Cu1···Cu2	4.164	0.03
	4.749	0.01
	4.757	0.01
	5.861	1.00[a]
Cu2···Cu2	4.771	0.04
	5.251	0.54
	5.792	0.11
	5.817	0.11

[a] $(\Delta e)^2 = 47500$ $(meV)^2$.

The geometrical parameters associated with various SSE paths of $SrCu_2(PO_4)_2$ are summarized in Table 4, and the relative $(\Delta e)^2$ values calculated for the SE and SSE paths are given in Table 5. Our calculations for the SSE interactions were carried out with and without the PO_4 units associated with the O···O contacts. Table 5 shows those calculated without including the PO_4 units associated with the O···O contacts. The SE interaction is negligible because the spin-exchange path Cu1−O−Cu2 is highly unsymmetrical. The two strongest SSE interactions in Table 5 form isolated linear tetramer units Cu1−Cu2−Cu2−Cu1, in which the Cu1−Cu2 and Cu2−Cu2 paths have one and two Cu−O···O−Cu linkages, respectively (Figure 5). The arrangement of the linear tetramer units is shown in Figure 4. To a first approximation, therefore, the magnetic structure of $SrCu_2(PO_4)_2$ may be described by a linear four-spin cluster (LFSC) model with two spin-exchange parameters J_1 and J_2, i.e., by the spin Hamiltonian

$$\hat{H}_{LFSC} = -2J_1(\hat{S}_1\hat{S}_2 + \hat{S}_3\hat{S}_4) - 2J_2\hat{S}_2\hat{S}_3 \qquad (1)$$

Our calculations for the SSE interactions including the PO_4 units associated with the O···O contacts provide similar

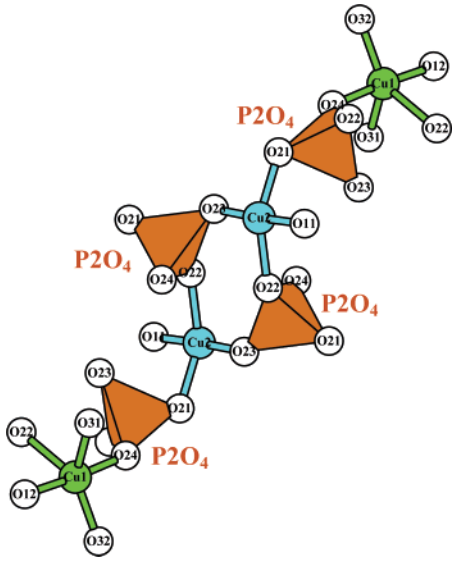

Figure 5. Schematic view of a Cu1−Cu2−Cu2−Cu1 linear four-spin cluster made up solely of Cu−O···O−Cu super-superexchange paths.

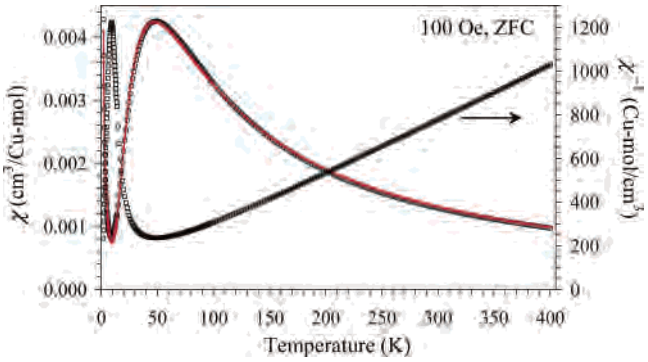

Figure 6. $\chi(T)$ and $\chi^{-1}(T)$ curves for $SrCu_2(PO_4)_2$ (symbols) as a function of temperature. The bold solid line on the $\chi^{-1}(T)$ curve is the fit to eq 2 at 150−400 K. The bold solid line for the $\chi(T)$ curve is the fit using the linear four-spin cluster model (eqs 5 and 7) in the 2−400 K region. The parameters of the fitting are presented in Table 6.

trends. In general, the magnetic orbital of a CuO_n ($n = 5, 6$) unit is the highest-lying d-block level, which is σ-antibonding in nature between the Cu 3d and oxygen 2p orbitals. Thus, the magnetic orbital is contained in the CuO_4 unit made up of the shortest four Cu−O bonds of a CuO_n unit, and the strength of a SSE interaction increases with the increasing ∠Cu−O···O angle and the decreasing O···O distance. This is the reason why the SSE path with Cu1···Cu2 = 5.861 Å is very strong.

3.4. Magnetic Properties of $SrCu_2(PO_4)_2$. A. Magnetic Susceptibility. Figure 6 presents plots of χ and χ^{-1} (ZFC curves) against the temperature, T, recorded for $SrCu_2(PO_4)_2$ at 100 Oe. No noticeable difference was found between the curves measured under the ZFC and FC conditions. Also, no difference was observed between curves recorded at 100 and 5000 Oe, except for the lowest-temperature range where the $\chi(T)$ curves are dominated by impurities or defects. The high-temperature regions (150−400 K) were fitted very well by the modified Curie−Weiss law

$$\chi(T) = \chi_0 + \mu_{\text{eff}}{}^2 N(3k_B(T-\theta))^{-1} \qquad (2)$$

Table 6. Fitted Parameters for $\chi^{-1}(T)$ and $\chi(T)$ of $SrCu_2(PO_4)_2$

eq	quantity	$SrCu_2(PO_4)_2$
2	temp range (K)	150−400
	χ_0 (cm³/Cu mol)	$-6.9(3) \times 10^{-5}$
	μ_{eff} (μ_B)	1.895(4)
	θ (K)	−30.8(7)
5, 6	temp range (K)	2−400
dimer model	χ_0 (cm³/Cu mol)	$1.38(12) \times 10^{-4}$
	C_{imp} (cm³ K/Cu mol)	$5.17(13) \times 10^{-3}$
	θ_{imp} (K)	0.72(4)
	g	2.020(6)
	$-2J/k_B = \Delta/k_B$ (K)[b]	75.4(3)
	R[a]	9.10×10^{-4}
5, 7	temp range (K)	2−400
linear four-spin cluster model	χ_0 (cm³/Cu mol)	$-1.05(15) \times 10^{-4}$
	C_{imp} (cm³ K/Cu mol)	$6.54(12) \times 10^{-3}$
	θ_{imp} (K)	0.44(3)
	g	2.219(4)
	$-2J_1/k_B$ (K)	82.4(6)
	$-2J_2/k_B$ (K)	59(2)
	$\Delta_1/k_B = E_4 - E_6$ (K)[b]	63.1
	$\Delta_2/k_B = E_2 - E_6$ (K)[b]	101.7
	R[a]	3.33×10^{-4}
5 (this work), 56 (ref 37)	temp range (K)	2−400
bond-alternating linear chain model	χ_0 (cm³/Cu mol)	$-1.6(1) \times 10^{-4}$
	C_{imp} (cm³ K/Cu mol)	$6.77(10) \times 10^{-3}$
	θ_{imp} (K)	0.41(3)
	g	2.262(8)
	$-2J_1/k_B$ (K)	80.9(3)
	$\alpha = J_2/J_1$	0.494(7)
	R[a]	2.58×10^{-4}

[a] $R = \Sigma_{i=1}^{N_p}(\chi(T_i) - \chi_{\text{fit}}(T_i))^2/\Sigma_{i=1}^{N_p}(\chi(T_i))^2$. [b] Δ is a spin gap.

where χ_0 is the temperature-independent term, μ_{eff} is the effective magnetic moment, N is Avogadro's number, k_B is Boltzmann's constant, and θ is the Weiss constant, with the fitted parameters (χ_0, μ_{eff}, and θ) given in Table 6. The μ_{eff} value corresponds to a g factor of 2.19, which is typical for the Cu^{2+} ion. The negative Weiss constant suggests an antiferromagnetic interaction between the Cu^{2+} ions.

Below about 150 K, the deviation from the Curie−Weiss law was observed with a broad maxima on the $\chi(T)$ curve at $T_M = 48$ K, which is typical for low-dimensional Heisenberg antiferromagnets. Below T_M, the magnetic susceptibility decreases rapidly, which is characteristic of a spin-gapped behavior. The lowest-temperature region (below about 10 K) was characterized by an increase in the χ values from the presence of impurities or defects.

Spin-gapped behavior is predicted from several spin−structure models, which include a LFSC model (eq 1) as well as an isolated dimer and a bond-alternating linear chain (BALC) model, whose spin Hamiltonians are written as

$$\hat{H}_{\text{dimer}} = -2J\hat{S}_1\hat{S}_2 \qquad (3)$$

$$\hat{H}_{\text{BALC}} = -2\sum_n (J_1\hat{S}_{2n-1}\hat{S}_{2n} + J_2\hat{S}_{2n}\hat{S}_{2n+1}) \qquad (4)$$

In the whole range of temperatures, 2−400 K, the $\chi(T)$ data were fitted by the model

$$\chi(T) = \chi_0 + C_{\text{imp}}/(T - \theta_{\text{imp}}) + \chi_{\text{spin}}(T) \qquad (5)$$

where C_{imp} is an impurity Curie constant and θ_{imp} is an impurity Weiss constant. For the dimer model, the $\chi_{\text{spin}}(T)$

term is given by

$$\chi_{spin}(T) = \chi_{dimer}(T) = Ng^2\mu_B{}^2(k_BT)^{-1}(3 + \exp(-2J/(k_BT)))^{-1} \quad (6)$$

where g is the g factor and $-2J$ is the spin-exchange parameter for the dimer unit. However, as shown in Table 6, this dimer model does not provide a good fit and leads to a very small value for g (i.e., 2.02) compared with $g = 2.24$ obtained from the EPR experiments for $SrCu_2(PO_4)_2$. Note that $SrCu_2(PO_4)_2$ gave the isotropic line shape even in the high-field ESR measurement at 160 GHz; in other words, the anisotropic g values could not be resolved. In addition, the spin gap of the dimer model was larger than the experimental spin gap (75 K vs 65 K). These facts indicated that the dimer model is incorrect. We then tried to include the inter-dimer interaction (zJ') with a mean-field approximation. Nevertheless, it hardly improved the fit, as the R factors indicate (see Supporting Information). In addition, the fits gave the large values of zJ'/k_B apparently beyond the validity of a mean-field approximation ($|zJ'| \ll |J|$).

Then, we fitted the $\chi(T)$ data using the LFSC model (eqs 5 and 7),[36] for which $\chi_{spin}(T)$ is given by

$$\chi_{spin}(T) = \chi_{linear-tetramer}(T) =$$

$$\frac{Ng^2\mu_B{}^2}{4k_BT}\left[10\exp\left(-\frac{E_1}{k_BT}\right) + 2\exp\left(-\frac{E_2}{k_BT}\right) + 2\exp\left(-\frac{E_3}{k_BT}\right) + 2\exp\left(-\frac{E_4}{k_BT}\right)\right]\Big/\left[5\exp\left(-\frac{E_1}{k_BT}\right) + 3\exp\left(-\frac{E_2}{k_BT}\right) + 3\exp\left(-\frac{E_3}{k_BT}\right) + 3\exp\left(-\frac{E_4}{k_BT}\right) + \exp\left(-\frac{E_5}{k_BT}\right) + \exp\left(-\frac{E_6}{k_BT}\right)\right] \quad (7)$$

where the energies E_i ($i = 1-6$) of the spin Hamiltonian, $\hat{H}$, in eq 1 are given by

$$E_1\,(S = 2) = -J_1 - J_2/2$$
$$E_2\,(S = 1) = J_1 - J_2/2$$
$$E_3\,(S = 1) = J_2/2 + \sqrt{J_1{}^2 + J_2{}^2}$$
$$E_4\,(S = 1) = J_2/2 - \sqrt{J_1{}^2 + J_2{}^2}$$
$$E_5\,(S = 0) = J_1 + J_2/2 + \sqrt{4J_1{}^2 - 2J_1J_2 + J_2{}^2}$$
$$E_6\,(S = 0) = J_1 + J_2/2 - \sqrt{4J_1{}^2 - 2J_1J_2 + J_2{}^2} \quad (8)$$

This fitting leads to a satisfactory result (Figure 6), and the fitting parameters are summarized in Table 6. The results of the fitting the $\chi(T)$ data using the BALC model (i.e., eq 5 with $\chi_{spin}(T)$ expressed by eq 56 in ref 37) are also summarized in Table 6. Both the LFSC and the BALC models fit the experimental data with similar quality, as can be seen from the R factors (Table 6). The results of the fitting using the BALC model are given to demonstrate that it is difficult to state which model is better solely on the basis of fitting the magnetic susceptibility data. For example, the BALC model is found if one considers the SE and the strongest SSE interaction with Cu1···Cu2 = 5.861 Å.

For $SrCu_2(PO_4)_2$, the spin gap deduced from the BALC model is 52 K[37] and that from the LFSC model is 63 K (i.e., the first exited energy $\Delta_1/k_B = E_4 - E_6$). The latter is in good agreement with the Cu NQR results (see below). With the strong support from the spin-dimer analysis, we conclude that the LFSC model provides a better description of the magnetism of $SrCu_2(PO_4)_2$. It is noted that the spin gap found from the ^{31}P NMR was much smaller ($\Delta_1/k_B = 47$ K).[11] Inelastic neutron scattering experiments[38] with oriented crystals would provide definitive information about the excitation spectrum of $SrCu_2(PO_4)_2$. The ratio J_2/J_1 of 0.72 obtained by fitting the $\chi(T)$ data using the LFSC model is in reasonable agreement with the prediction by the spin-dimer analysis ($J_2/J_1 = 0.54$) in view of the fact that the LFSC model was obtained by neglecting a number of other nonzero spin-exchange interactions (Table 5). In ref 11, the ratio $J_2/J_1 = 1.33$ was reported for the LFSC model.

B. ^{63}Cu NQR. Figure 7 depicts the ^{63}Cu nuclear spin lattice relaxation rates, $1/T_1$, measured for the two different Cu sites of $SrCu_2(PO_4)_2$. Because there are two nonequivalent Cu sites in $SrCu_2(PO_4)_2$, four NQR lines are observed under zero magnetic field for the presence of the two isotopes ^{63}Cu and ^{65}Cu. Measurements were done for the ^{63}Cu NQR lines at 31.31 MHz (low-frequency line) and 45.50 MHz (high-frequency line). Below about 12 K, a nonexponential recovery of ^{63}Cu nuclear magnetization was observed, which is probably caused by the existence of paramagnetic spins. The effect of impurity relaxation was parametrized by the relaxation rate, $1/\tau_1$, which was found to be almost temperature independent. The intrinsic relaxation rate, $1/T_1$, exhibits an activated temperature dependence reflecting a finite spin gap. The two Cu sites have essentially (at sufficiently low temperatures) the same spin-gap energy of about 65 K, although the $1/T_1$ data for the Cu site corresponding to the low-frequency line can be fitted with a slightly larger spin-gap value.

The spin gaps deduced from the Cu NQR and magnetization data (see below) are different. The discrepancy should be attributed in part to intercluster interactions. Since the intercluster interactions are weaker than the intracluster ones, low-field measurements, such as the magnetic susceptibility and Cu NQR, are insensitive to the intercluster interactions.[39] As a result, the $\chi(T)$ data can be fitted well with the four-spin cluster model. However, the high-field measurements, such as the magnetization, are sensitive to the intercluster interactions. For example, in $CaCuGe_2O_6$ with slightly interacting dimers, the shift in 9 T was observed between the experimental M vs H curve and the calculated one for

(36) Papadopoulos, A. N.; Tangoulis, A.; Raptopoulou, C. P.; Terzis, A.; Kessissoglou, D. P. *Inorg. Chem.* **1996**, *35*, 559.
(37) Johnston, D. C.; Kremer, R. K.; Troyer, M.; Wang, X.; Klümper, A.; Bud'ko, S. L.; Panchula, A. F.; Canfield, P. C. *Phys. Rev. B* **2000**, *61*, 9558−9606.
(38) Hase, M.; Etheredge, K. M. S.; Hwu, S.-J.; Hirota, K.; Shirane, G. *Phys. Rev. B* **1997**, *56*, 3231.

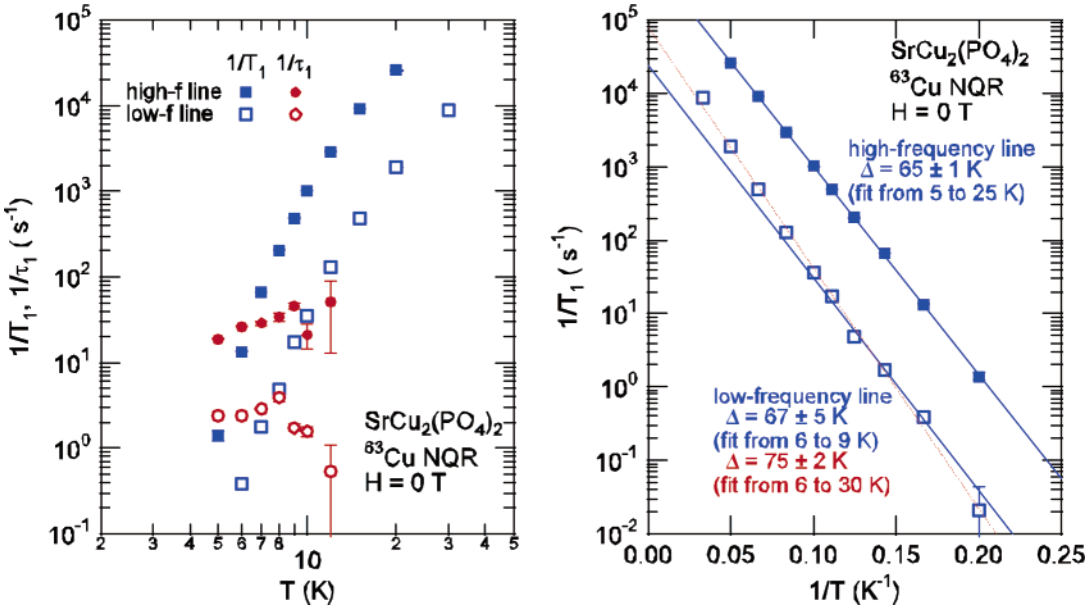

Figure 7. ^{63}Cu nuclear spin lattice relaxation rate, $1/T_1$, of $SrCu_2(PO_4)_2$ as a function of temperature (left) and reciprocal temperature (right).

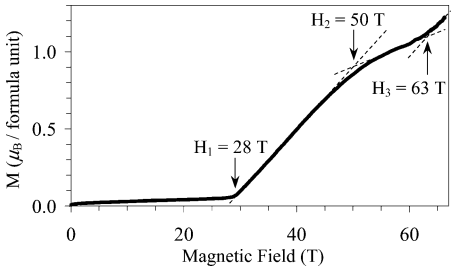

Figure 8. High-field magnetization curve for $SrCu_2(PO_4)_2$ at 1.3 K.

the isolated dimer.[9,39] The magnetic susceptibilities of $Sr_2Cu(BO_3)_2$ could be fitted well by the isolated dimer model.[40] However, the experimental high-field M vs H curves of $Sr_2Cu(BO_3)_2$ showed deviations from the isolated dimer model caused by interdimer interactions.[40] On the other hand, the interdimer interaction in $SrCu_2(BO_3)_2$ is very large ($J'/J = 0.64$)[41] and both the magnetic susceptibility and the high-field magnetization deviated greatly from the isolated dimer model.[10]

C. Magnetization. High-field isothermal magnetization data, M vs H, at 1.3 K are presented in Figure 8. The small change of the magnetization below about 30 T is caused by the presence of paramagnetic impurities. Above $H_1 \approx 28$ T, the magnetization rapidly increases and changes almost linearly with the field. The spin gap can be estimated using the equation

$$\Delta_1/k_B = 0.6714 g H_1 \qquad (9)$$

This equation gives $\Delta_1/k_B \approx 42$ K. The M vs H curve for $SrCu_2(PO_4)_2$ clearly shows a curvature near $H_2 = 50$ T with the magnetization value of about half the expected saturation value. Above $H_3 \approx 63$ T, the magnetization again tends to increase linearly with the field. These data indicate the existence of a 1/2-magnetization plateau. The appearance of a magnetization plateau may be related to intercluster interactions.

D. Specific Heat. The specific heat data exhibit no anomaly characteristic of a long-range ordering except for a very small peak at 0.9 K resulting from the long-range magnetic ordering in the impurity, $Sr_3Cu_3(PO_4)_4$.[42] These data show that $SrCu_2(PO_4)_2$ does not undergo long-range magnetic transitions down to 0.45 K. This fact is in accordance with the spin-singlet ground state for $SrCu_2(PO_4)_2$ found by the Cu NQR and high-field magnetization measurements.

4. Concluding Remarks

In summary, we have successfully determined the crystal structure of $SrCu_2(PO_4)_2$ from synchrotron XRD data. The magnetic properties of $SrCu_2(PO_4)_2$ were characterized by magnetic susceptibility, high-field magnetization, Cu NQR, ESR, and specific heat measurements, and the structural properties were characterized by Raman spectroscopy. $SrCu_2(PO_4)_2$ crystallizes in a new structure type with the $Cu1Cu2O_8$ structural dimers consisting of the Cu1−O−Cu2 superexchange path. From the magnetic point of view, however, the magnetic properties of $SrCu_2(PO_4)_2$ are described by Cu1−Cu2−Cu2−Cu1 linear four-spin clusters made up solely of Cu−O···O−Cu super-superexchange paths.

Acknowledgment. The authors express their thanks to the Ministry of Education, Culture, Sports, Science and Technology, Japan, for Grant-in-Aid No. 12CE2005, for COE Research on Elements Science (Nos. 13440111 and 14204070), and for 21COE on the Kyoto Alliance for Chemistry. ICYS is supported by Special Coordination Funds

(39) Sasago, Y.; Hase, M.; Uchinokura, K.; Tokunaga, M.; Miura, N. *Phys. Rev. B* **1995**, *52*, 3533.
(40) Sebastian, S. E.; Yin, D.; Tanedo, P.; Jorge, G. A.; Harrison, N.; Jaime, M.; Mozharivskyj, Y.; Miller, G.; Krzystek, J.; Zvyagin, S. A.; Fisher, I. R. *Phys. Rev. B* **2005**, *71*, 212405.
(41) Kodama, K.; Takigawa, M.; Horvatic, M.; Berthier, C.; Kageyama, H.; Ueda, Y.; Miyahara, S.; Becca, F.; Mila, F. *Science* **2002**, *298*, 395.
(42) Belik, A. A.; Matsuo, A.; Azuma, M.; Kindo, K.; Takano, M. *J. Solid State Chem.* **2005**, *178*, 709.

for Promoting Science and Technology from MEXT, Japan. M.-H.W. thanks the Office of Basic Energy Sciences, Division of Materials Sciences, U.S. Department of Energy for the financial support under Grant DE-FG02-86ER45259.

Supporting Information Available: DTA curve for $SrCu_2(PO_4)_2$ (Figure S1), Raman spectrum of $SrCu_2(PO_4)_2$ at room temperature (Figure S2), absorption line observed at 160 GHz for $SrCu_2(PO_4)_2$ in X-band ESR measurement (Figure S3), the results of the fitting of the $\chi(T)$ data by the dimer model (Figure S4), $C_p(T)$ curve for $SrCu_2(PO_4)_2$ (Figure S5), bond valence sum calculations for $SrCu_2(PO_4)_2$ (Table T1), the results of the fitting of the $\chi(T)$ data by the dimer model with interdimer interactions using a mean-field approximation (Table T2) (PDF). This material is available free of charge via the Internet at http://pubs.acs.org.

IC051079H